JOURNAL OF Materials CHEMISTRY

Reaction mechanism and kinetics analysis of lithium nickel oxide during solid-state reaction

Chung-Hsin Lu* and Lee Wei-Cheng

Department of Chemical Engineering, National Taiwan University, Taipei, Taiwan, R.O.C.

Received 18th November 1999, Accepted 8th March 2000
Published on the Web 25th April 2000

The reaction mechanism and kinetics analysis for the formation of lithium nickel oxide ($LiNiO_2$) during solid-state reaction have been investigated. The atmosphere during the reaction has a pronounced effect on the stoichiometry and cation arrangement of $LiNiO_2$. It is obligatory to supply adequate oxygen partial pressure to overcome the diffusion barrier existent in the precursor powder. It is difficult to synthesize stoichiometric $LiNiO_2$ with the $R\bar{3}m$ structure if the oxygen partial pressure is too low. The formation of $LiNiO_2$ requires continuous heat treatment for a certain period of time which depends on the heating temperature and the oxygen partial pressure provided. Based on the Johnson–Mehl–Avrami equation, $LiNiO_2$ formation is governed by a three-dimensional diffusion controlled mechanism. The reaction kinetics of $LiNiO_2$ formation are satisfactorily expressed by the Brounshtein–Ginstling model, and the activation energy of the formation process is estimated to be 76.1 kJ mol^{-1}. A microscopic reaction model for the formation of $LiNiO_2$ has been established.

Introduction

In recent years, due to the development and popularity of portable electronic devices, the demand for rechargeable batteries with high voltage and high energy density has increased. Four volt secondary lithium ion batteries have evoked great interest among battery researchers because of their high energy density, long cycle life, and moderate rate capabilities.[1–4] Lithium nickel oxide ($LiNiO_2$) is a very promising positive electrode material for rechargeable lithium ion batteries among such materials as $LiCoO_2$ and $LiMn_2O_4$. The reversible specific capacity reported by most groups falls into the 120–140 mA h g^{-1} range.[5–7] The reported rechargeable capacity of $LiMn_2O_4$ is less than that of $LiCoO_2$, around 110 mA h g^{-1},[8,9] while for $LiNiO_2$ it is comparable to that for $LiCoO_2$.[1,10] Furthermore, using $LiNiO_2$ as an electrode material is more attractive than $LiCoO_2$ from the natural source availability and cost effectiveness points of view.[11–13] In comparison with $LiMn_2O_4$, $LiNiO_2$ has greater reversible capacity. Consequently, $LiNiO_2$ is very competitive for use as an electrode material in four volt secondary lithium ion batteries.

$LiNiO_2$ exhibits a hexagonal symmetry with an $R\bar{3}m$ space group in which lithium ions and nickel ions are situated in 3a and 3b sites and oxygen ions in 6c sites.[3] In the $R\bar{3}m$ structure of $LiNiO_2$, 3a and 3b sites are equivalent to the oxygen ion close packed cubic octahedral sites. With these sites occupied, a layered framework is constructed. The layered structure of $LiNiO_2$ provides a two-dimensional route for lithium intercalation and de-intercalation. The stoichiometry of $LiNiO_2$ significantly affects the $LiNiO_2$ performance.[14–16] However, stoichiometric $LiNiO_2$ is difficult to synthesize, because high temperature treatment of $LiNiO_2$ causes lithium ions to volatilize, resulting in non-stoichiometric $LiNiO_2$. The lithium ion deficiency will lead to a structural disorder in the $LiNiO_2$ matrix, impeding the lithium ion intercalation and de-intercalation. The non-stoichiometric phenomenon existing in the $LiNiO_2$ matrix curtails the utilization of lithium ions and leads to cell electrochemical performance deterioration.[3] The stoichiometry and order–disorder behavior of $LiNiO_2$ were reported to be related to the relative integrated intensities of the X-ray diffraction lines.[2,17,18]

$LiNiO_2$ powder is usually prepared in a solid-state reaction by heating intimately mixed lithium and nickel salts at elevated temperatures. In the heating processes of ceramic systems, the preliminary product is produced at the interface. As the reaction continues, the reactants diffuse through the product shell and react with the unreacted core. Although the electrochemical properties of $LiNiO_2$ have been intensively explored, the formation mechanism and reaction kinetics of $LiNiO_2$ have not been studied. The details related to the reaction process are crucial for controlling the heating conditions to obtain a monophasic powder that has a homogeneous microstructure and fine grain size. The aim of this work is to elucidate the reaction mechanism and reaction kinetics of $LiNiO_2$ in a solid-state reaction. First, the reaction conditions for the synthesis of $LiNiO_2$ are investigated for studying the optimum reaction temperature range and the oxygen stream flow rate required for $LiNiO_2$ to form. Second, the $LiNiO_2$ reaction kinetics are analyzed based on the relationship between the conversion ratio and reaction time during isothermal heating. The control step for the formation of $LiNiO_2$ is then determined. In addition, from microstructural observations accompanied with the kinetics analysis, a reaction model for the solid-state reaction of $LiNiO_2$ is established.

Experimental procedure

Stoichiometric Li_2CO_3 and NiO in a molar ratio 1 : 2 were ball-milled for 48 h with ethyl alcohol as the dispersion agent, using zirconia balls in a polyethylene (PE) jar. The well-mixed powder was dried in a rotary evaporator. The dried powder was then pressed into 8 mm-diameter pellets before reaction. Heating the pellets in an electrical furnace induced the $LiNiO_2$ formation. In order to better understand the effect of partial oxygen pressure on the reaction; the oxygen flow rate was varied from 0 to 2000 ml min^{-1}.

The differential thermal analysis and thermogravimetric analysis (DTA–TG) were performed under an oxygen stream with a flow rate of 100 ml min^{-1} from room temperature to 800 °C, at a heating rate of 10 °C min^{-1} to measure the reaction and starting material weight loss. For the isothermal-heating

DOI: 10.1039/a909130k

experiments, the heating temperatures were 750 °C, 800 °C, and 850 °C. The heating time was prolonged up to 140 min. The heated samples were quenched by quickly removing them from the furnace and immediately cooling to room temperature, they were then ground into a fine powder to perform the X-ray diffraction (XRD) analysis. XRD patterns of the samples were obtained with an X-ray diffractometer using CuKα radiation. Scanning electron microscopy (SEM) was performed to observe the microstructure of the calcined samples.

Results and discussion

Thermal analysis and X-ray powder diffraction study

The DTA–TG curves recorded for the mixed powders from room temperature to 800 °C are shown in Fig. 1. The DTA measurement indicates two endothermic peaks at around 70 °C and 720 °C, and one exothermic peak at around 310 °C. The endothermic peak at 70 °C, with a slight weight loss, is believed to be attributable to the evaporation of residual ethylene alcohol from the mixed powders. The exothermic peak at 310 °C, accompanied by a relatively steeper weight loss curve, was caused by the combustion of the PE bits from the PE jar during ball-milling. In order to explain the endothermic peak beginning at 710 °C, another DTA–TG analysis for pure lithium carbonate was also performed. Lithium carbonate was found to melt and decompose to evolve into carbon dioxide at about 710 °C.[19] As a result, the sharp and strong endothermic peak beginning at 710 °C, accompanied by the greatest weight loss rate, is attributed to the decomposition and melting of Li_2CO_3. The impurity weight percentage (PE bits) in the mixed powders was equivalent to the weight loss percentage before the decomposition of Li_2CO_3. From the TGA curve, it was estimated to be 2.2%.

As shown in Fig. 4 (later), no intermediate compounds are produced during the formation of $LiNiO_2$. Therefore, the formation of $LiNiO_2$ can be represented by the following equation:

$$NiO+\frac{1}{2}Li_2CO_3+\frac{1}{4}O_2\rightarrow LiNiO_2+\frac{1}{2}CO_2 \quad (1)$$

Because oxygen participates in eqn. (1), the oxygen flow rate is speculated to play an important role in the formation of $LiNiO_2$. It was reported that the oxygen flow rate significantly influenced the stoichiometry of $LiNiO_2$, and insufficient oxygen flow rate results in a deficiency of lithium in $LiNiO_2$.[20] Therefore, the minimum oxygen flow rate supplying sufficient oxygen partial pressure to overcome the diffusion barrier of the solid pellets should be determined in case the non-stoichiometry of $LiNiO_2$ occurs due to an insufficiency in the oxygen supply. The starting powder was heated under oxygen streams of various flow rates at 800 °C for 2 h. Fig. 2 illustrates the oxygen flow rate influence on the $LiNiO_2$ synthesis reaction. When the reaction was carried out under ambient atmosphere, the $R\bar{3}m$ structure of $LiNiO_2$ did not form as shown in Fig. 2(a). The product exhibited the cubic structure reported by Reimers *et al.*,[21] and this structure leads to poor electrical properties.[2] As the oxygen stream flow rate was increased to 500 ml min^{-1}, the $R\bar{3}m$ structure appeared (Fig. 2(b)). This XRD pattern is characteristic of the electrochemically active $LiNiO_2$ described by Ohzuku *et al.*[2] If the oxygen flow rate was increased further up to 1000 ml min^{-1}, the X-ray diffraction line intensity also increased (Fig. 2(c)), suggesting that higher crystallinity could be achieved by increasing the oxygen stream flow rate to 1000 ml min^{-1}. At an oxygen flow rate of 2000 ml min^{-1}, no further amelioration of crystallinity was observed (Fig. 2(d)). The diffraction intensities shown in Fig. 2(d) are very close to those in Fig. 2(c). According to the above results, an oxygen stream with a flow rate of 1000 ml min^{-1} was found to supply sufficient oxygen partial pressure required for the $LiNiO_2$ synthesis reaction. Therefore, the following kinetic experiments were carried out under this condition.

Reaction kinetic analysis

The $LiNiO_2$ conversion ratio can be calculated from the weight loss data in eqn. (1), which results in a starting pellet net weight loss of 12.54%. The weight loss is caused by the weight difference between the evolved CO_2 and the O_2 supplied by the environment. The $LiNiO_2$ conversion ratio is defined as x ($0\leqslant x\leqslant 1$) and can be expressed as

$$x=\frac{\Delta W_{\text{true}}\%}{12.54\%} \quad (2)$$

We define

$$\Delta W_{\text{true}}\%=\frac{\Delta W-0.022W_{\text{i}}}{0.978W_{\text{i}}}\times 100\%$$

where $\Delta W_{\text{true}}\%$ is the weight loss percentage caused by the evolved CO_2, ΔW is the weight difference before and after the reaction, W_{i} is the weight of the starting pellet, $0.022W_{\text{i}}$ is the weight of the PE bits contained in the pellet, and $0.978W_{\text{i}}$ is the true weight of the mixed Li_2CO_3 and NiO powders.

As deduced from Fig. 1, for the reaction to proceed, the temperature must be higher than 710 °C. Therefore, the chosen reaction temperatures were 750 °C, 800 °C, and 850 °C. The mixed $LiNiO_2$ precursors were isothermally heated at these three temperatures for various periods of time and then

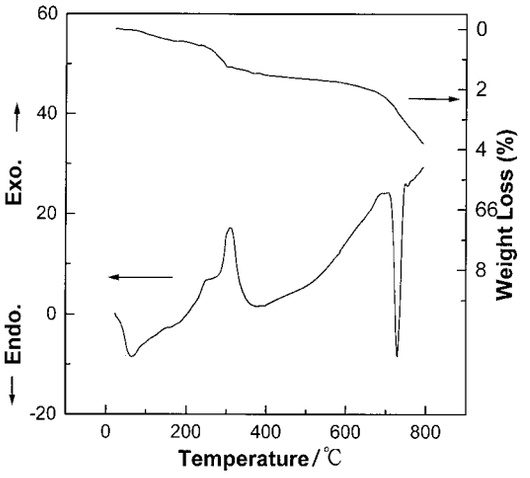

Fig. 1 Differential thermal analysis and thermogravimetry analysis of the starting materials of $LiNiO_2$.

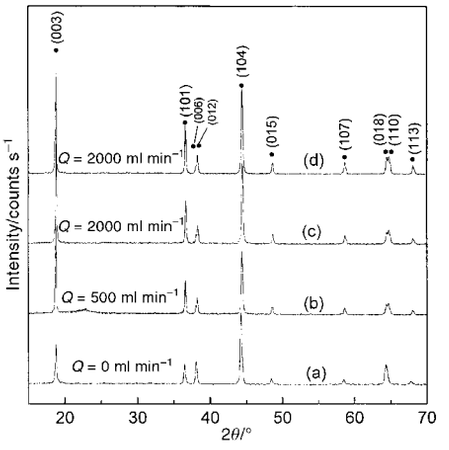

Fig. 2 X-Ray diffraction patterns of $LiNiO_2$ samples prepared at 800 °C for 2 h under oxygen streams of various flow rates.

quenched to room temperature. The weight difference ΔW of each specimen before and after the heating process was recorded. The $LiNiO_2$ conversion ratio at each heating condition was calculated using eqn. (2). Fig. 3 illustrates the relationship between the conversion ratio and heating time at these three temperatures. At all of the three temperatures, the longer the heating time, the higher the conversion ratio. Heating specimens at 750 °C for 100 min increased the conversion ratio to about 59%. When the temperature was raised to 850 °C, the same heating time resulted in a near 85% conversion ratio. If the heating time was prolonged to 140 min at 850 °C, the conversion ratio could be as high as 90%. Either raising the reaction temperature or prolonging the heating time led to an increase in the conversion ratio.

Fig. 4 shows the results of X-ray diffraction patterns for samples quenched at different heating times during isothermal heating at 850 °C. When the specimen was quenched before the onset of isothermal heating, only NiO and Li_2CO_3 could be observed in the XRD pattern. This indicates that no reaction took place. As the heating time proceeded, $LiNiO_2$ started to form. The (003) and (101) $LiNiO_2$ diffraction lines appeared after heating for 20 min. As the heating time increased, the $LiNiO_2$ diffraction lines became sharper and stronger. The XRD pattern of the specimen heated for 140 min exhibited the characteristics of electrochemically active $LiNiO_2$.

In order to determine the proper function to describe the reaction behavior of eqn. (1), the Johnson–Mehl–Avrami equation[22]

$$x = 1 - \exp(-rt^m) \tag{3}$$

is introduced, where x is the conversion ratio, t is the reaction time and m is a constant that depends upon the reaction mechanism. With proper linearization processes, eqn. (3) can be written as:

$$\ln[-\ln(1-x)] = \ln(r) + m\ \ln(t) \tag{4}$$

By substituting the conversion ratio data in Fig. 3 into eqn. (4), one can make a plot of the regression lines of eqn. (4) at the three reaction temperatures, as shown in Fig. 5. The data points for each temperature were perfectly linearly dependent. The three regression lines were almost parallel, and their slopes were 0.579, 0.576, and 0.581, respectively. They were very close to each other, implying that the reactions occurring in the studied temperature ranges were governed by a single reaction mechanism. Comparing the m values with the reaction mechanisms collected by Sharp *et al.*,[23] it is reasonable to conclude that the $LiNiO_2$ formation reaction mechanism is a three-dimensional diffusion controlled process ($m = 0.57$). Therefore, the relation between the conversion ratio (x) and the reaction time (t) for this mechanism can be expressed by the Brounshtein–Ginstling model:[24]

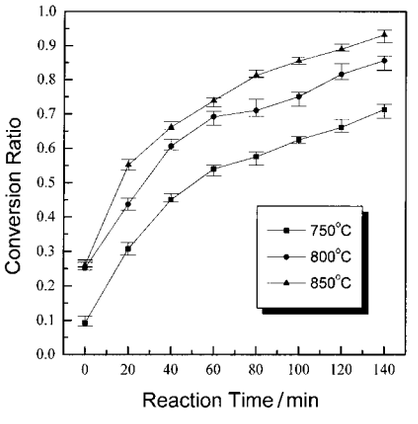

Fig. 3 Relationship between conversion ratio (x) and reaction time (t) during isothermal heating at 750 °C , 800 °C, and 850 °C.

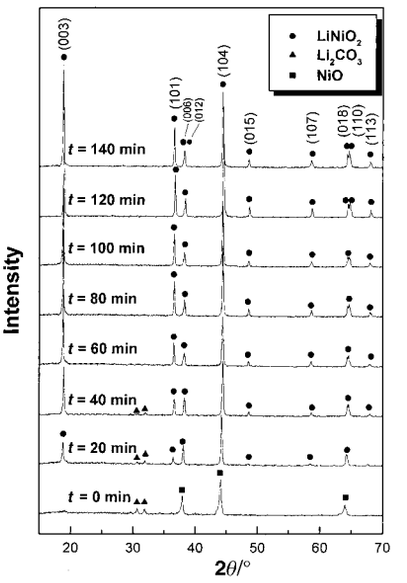

Fig. 4 X-Ray diffraction patterns for $LiNiO_2$ samples heated at 850 °C for various heating times.

$$1 - 2x/3 - (1-x)^{2/3} = kt \tag{5}$$

The plot of $1-2x/3-(1-x)^{2/3}$ *versus* the reaction time t at each reaction temperature is illustrated in Fig. 6. The reaction rate constant, k, at each reaction temperature was obtained from the slope of the plot. Fig. 6 shows that all three lines have good linearity. Therefore, the Brounshtein–Ginstling model can correctly describe the $LiNiO_2$ formation reaction mechanism. The reaction rate constant k values at 750 °C, 800 °C, and 850 °C were $6.2 \times 10^{-4}\ min^{-1}$, $1.01 \times 10^{-3}\ min^{-1}$ and $1.4 \times 10^{-3}\ min^{-1}$, respectively. The activation energy (E) of the reaction was estimated by the Arrhenius equation:

$$k = k_0\ \exp(-E/RT) \tag{6}$$

where k is the reaction rate constant, E is the activation energy, R is the gas constant. T is the temperature. The graph of ln (k) *versus* $1/T$ is given in Fig. 7. From this plot, the activation energy of $NiO + \frac{1}{2}Li_2CO_3 + \frac{1}{4}O_2 \rightarrow LiNiO_2 + \frac{1}{2}CO_2$ was evaluated to be 76.1 kJ mol^{-1}, and the value of k_0 was 4.15 min^{-1}.

Microstructural observation and reaction model

In order to observe the microstructural change in the specimens, SEM was performed. During the heating process, a liquid phase was observed, as shown in Fig. 8. Fig. 8(a) shows the microstructure of the starting pellet quenched at 700 °C. The

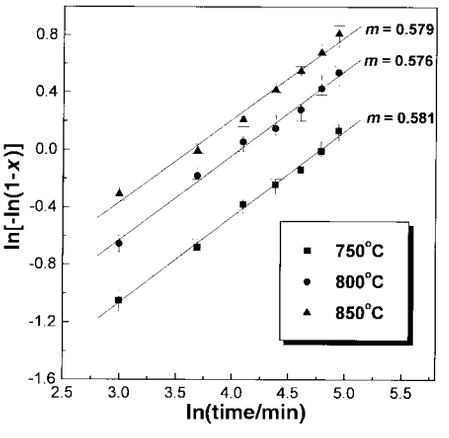

Fig. 5 Linear regression plot for $\ln[-\ln(1-x)]$ *versus* $\ln(t)$. x is the conversion ratio and t is the reaction time.

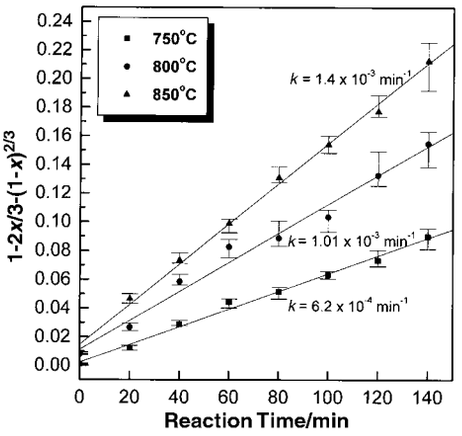

Fig. 6 Plot of $1-2x/3-(1-x)^{2/3}$ *versus* reaction time for the reaction process of $LiNiO_2$.

grains exhibited a clear particulate form. In the XRD analysis, only the starting materials were observed, indicating that there was no reaction occurring at 700 °C. Fig. 8(b) shows the microstructure of an 800 °C quenched sample, revealing that the melted substance enclosed solid particles. The existence of a liquid phase is believed to result from the melting of Li_2CO_3. The melting of Li_2CO_3 was found to occur at around 710 °C by DTA (Fig. 1), which is consistent with the SEM observations.

During Li_2CO_3 melting, the melted lithium species three-dimensionally diffused into nickel oxide resulting in the formation of $LiNiO_2$. The three-dimensional diffusion behavior is consistent with the primary premise in the Brounshtein–Ginstling model[24] used in the previous kinetic analysis. In the diffusion-controlled mechanism and microstructural variation view, a microscopic reaction model is proposed and illustrated in Fig. 9. First, the solid state lithium carbonate melts, becomes a liquid phase and then encloses the nickel oxide particles. Second, the melted lithium carbonate decomposes to escape the carbon dioxide. Then Ni^{2+} diffuses out from NiO into the melted lithium species to become Ni^{3+}, and Li^+ counter-diffuses into the octahedral-site vacancies in NiO created by the out-diffusion of Ni^{2+}. $LiNiO_2$ is formed through the rearrangement of cations in the oxygen ion close packed octahedral sites. Based on the above kinetic analysis and the proposed reaction model, the diffusion process of lithium and nickel species is realized to significantly determine the formation of $LiNiO_2$.

Conclusions

The reaction mechanism and kinetic analysis for the formation of $LiNiO_2$ were investigated in this study. Oxygen partial pressure was found to be a key factor having a significant effect on the reactions. For the formation of $LiNiO_2$ with $R\bar{3}m$ structure, flowing oxygen with a minimum flow rate of 1000 ml min^{-1} is required to overcome the diffusion barrier existing in the precursor powder. The conversion of $LiNiO_2$ from the starting materials increases with an increase in the heating temperature as well as heating time. From the reaction kinetic isothermal analysis, $LiNiO_2$ formation is confirmed to be governed by a three-dimensional diffusion controlled mechanism. Based on the Brounshtein–Ginstling model, the activation energy of the formation process is estimated to be 76.1 kJ mol^{-1}. In view of the diffusion controlled mechanism and microstructural observation, a microscopic reaction model for the formation of $LiNiO_2$ was proposed.

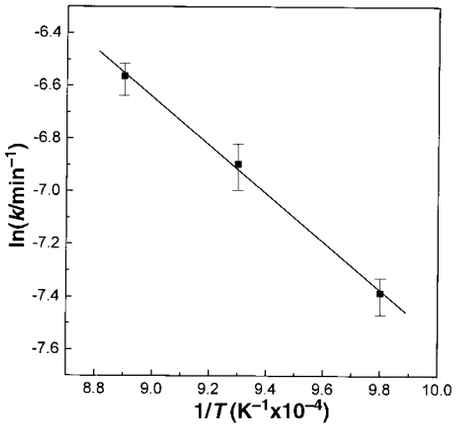

Fig. 7 Plot of $\ln(k)$ *versus* $1/T$ for the formation process of $LiNiO_2$.

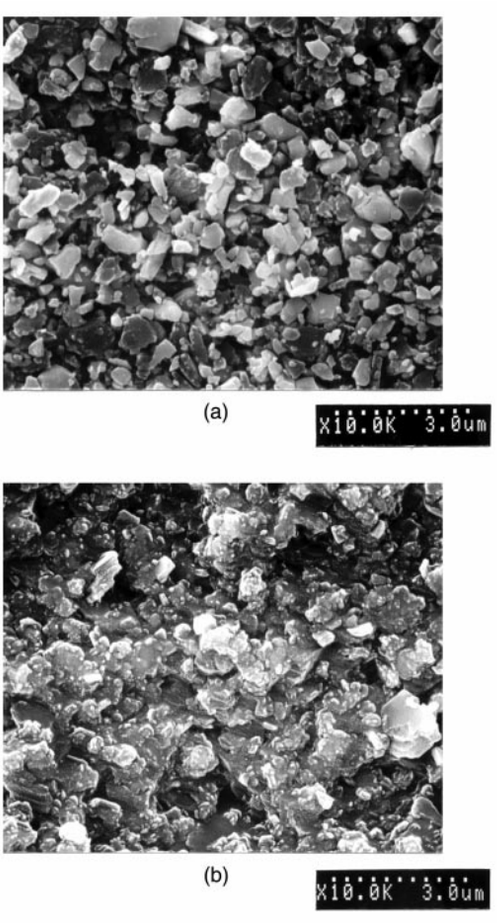

Fig. 8 Scanning electron micrographs of $LiNiO_2$ samples quenched at (a) 700 °C and (b) 800 °C.

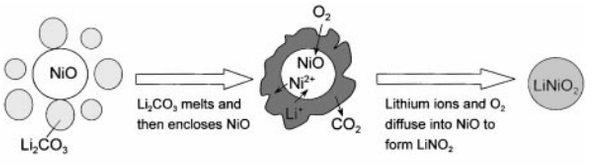

Fig. 9 A reaction model for the $LiNiO_2$ formation during solid-state reaction.

References

1 J. R. Dahn, U. von Sacken, M. W. Juzkown and H. Al-Janaby, *J. Electrochem. Soc.*, 1991, **138**, 2207.
2 T. Ohzuku, A. Ueda and M. Nagayama, *J. Electrochem. Soc.*, 1993, **140**, 1862.
3 W. Ebner, D. Fouchard and L. Xie, *Solid State Ionics*, 1994, **69**, 238.

4 M. Broussely, F. Perton, P. Biensan, J. M. Bodet, J. Labat, A. Lecerf, C. Delmas, A. Rougier and J. P. Peres, *J. Power Sources*, 1995, **54**, 109.
5 M. Antaya, J. R. Dahn, J. S. Preston, E. Rossen and J. N. Reimers, *J. Electrochem. Soc.*, 1993, **140**, 575.
6 M. Broussely, F. Perton, J. Labat, R. J. Staniewicz and A. Romero, *J. Power Sources*, 1993, **43–44**, 209.
7 K. Sekai, H. Azuma, A. Omaru, S. Fujita, H. Imoto, T. Endo, K. Yamaura, Y. Nishi, S. Mashiko and M. Yokogawa, *J. Power Sources*, 1993, **43–44**, 241.
8 I. Koetschau, M. N. Richard, J. R. Dahn J. B. Soupart and J. C. Rousche, *J. Electrochem. Soc.*, 1995, **142**, 2906.
9 J. M. Tarascon, E. Wang, F. K. Shokoohi, W. R. McKinnon and S. Colson, *J. Electrochem. Soc.*, 1991, **138**, 2859.
10 T. Ohzuku, A. Ueda, M. Nagayama, Y. Iwakoshi and K. Sawai, *Chem. Express*, 1992, **7**, 689.
11 S. Yamada, M. Fujiwara and M. Kanda, *Solid State Ionics*, 1996, **84**, 1.
12 Y. M. Choi, S. I. Pyun, S. I. Moon and Y. E. Hyung, *J. Power Sources*, 1995, **72**, 83.
13 M. Morita, O. Yamada, M. Ishikawa and Y. Matsuda, *J. Appl. Electrochem.*, 1998, **28**, 209.
14 H. Arai, S. Okada, Y. Sakurai and J. Yamaki, *Solid State Ionics*, 1997, **95**, 275.
15 A. Rougier, P. Gravereau and C. Delmas, *J. Electrochem. Soc.*, 1996, **143**, 1168.
16 J. P. Peres, C. Delmas, A. Rougier, M. Broussely, F. Perton, P. Biensan and P. Willmann, *J. Phys. Chem. Solids*, 1996, **57**, 1057.
17 J. N. Reimers, J. R. Dahn, J. E. Greedan, C. V. Stager, G. Liu, I. Davidson and U. von Sachen, *J. Solid State Chem.*, 1993, **102**, 542.
18 R. Moshtev, P. Zlatilova, V. Manev and K. Tagawa, *J. Power Sources*, 1996, **62**, 59.
19 A. Reisman, *J. Am. Chem. Soc.*, 1968, **80**, 3558.
20 D. Caurant, N. Baffier, B. Garcia and J. P. Perera-Ramos, *Solid State Ionics*, 1996, **91**, 45.
21 J. N. Reimers, W. Li and J. R. Dahn, *Phys. Rev. B*, 1993, **47**, 8486.
22 M. Avrami, *J. Chem. Phys.*, 1939, **7**, 1103.
23 J. H. Sharp, G. W. Brindley and B. N. Narahari Achar, *J. Am. Ceram. Soc.*, 1966, **49**, 379.
24 A. M. Ginstling and B. I. Brounshtein, *J. Appl. Chem. USSR (Engl. Transl.)*, 1950, **23**, 1327.